Title

Axial variation of deoxyhemoglobin density as a source of the low-frequency time lag structure in blood oxygenation level-dependent signals.

Authors

Toshihiko Aso[1,2*], Shinnichi Urayama[2,3], Fukuyama Hidenao[2,3], Toshiya Murai[1]

Affiliations

[1]Department of Psychiatry, Kyoto University Graduate School of Medicine, Kyoto, Japan

[2]Human Brain Research Center, Kyoto University Graduate School of Medicine, Kyoto, Japan

[3]Research and Educational Unit of Leaders for Integrated Medical System, Center for the Promotion of Interdisciplinary Education and Research, Kyoto University, Kyoto, Japan

* Correspondence:

Toshihiko Aso
aso.toshihiko@gmail.com

Keywords

BOLD contrast, Low-frequency oscillations, Cerebral blood flow, Neurovascular coupling, Resting-state fMRI, Image denoising

Abstract

Perfusion-related information is reportedly embedded in the low-frequency component of blood oxygen level-dependent (BOLD) fMRI signal. The blood-propagation pattern through the cerebral vascular tree is detected as an interregional lag variation of spontaneous low-frequency oscillations (sLFOs). Mapping of this lag, or phase, has been implicitly treated as a projection of the vascular tree structure onto real space. While accumulating evidence supports the biological significance of this signal component, the physiological basis of the "perfusion lag structure," a requirement for an integrative fMRI-signal model, is lacking. In this study, we conducted analyses furthering the hypothesis that the sLFO is not only largely of systemic origin, but also essentially intrinsic to blood and hence, behaves as a virtual tracer. By summing the small fluctuations of instantaneous phase differences between adjacent vascular regions, a velocity response to respiratory challenges was detected. Regarding the relationship to neurovascular coupling, the removal of the whole lag structure, which can be considered as an optimized global-signal regression, resulted in a reduction

of signal variance, while preserving the fMRI response. Examination of the T2* and S_0, or non-BOLD, components of the fMRI signal revealed that the lag structure is deoxyhemoglobin-dependent, while paradoxically presenting a signal-magnitude reduction in the venous side of the cerebral vasculature. These findings provide insight into the origin of BOLD sLFO, at least partly intrinsic to the circulating blood.

1 Introduction

In functional magnetic resonance imaging (fMRI), there are two established physiological bases of signal change: neuro-vascular coupling (NVC) and autoregulation. The former involves a local blood flow increase at 30-70% which gives rise to 0.5-2% blood oxygenation level-dependent (BOLD) signal increase with around 5-second delay (Buxton, 2013). This is the target phenomenon of fMRI as a tool for brain mapping, due to its limited spatial extent mainly involving local arterioles (Hillman, 2014). In contrast, autoregulatory response in vessel diameter is found in a wide range of arteries including internal carotid or middle cerebral arteries (Hoiland *et al.*, 2016). Detection of a compromised response in vascular disorders have been proven useful for clinical purpose (Murphy *et al.*, 2011). Importantly, there is no clear physiological distinction between these two phenomena each involving multiple pathways (Willie *et al.*, 2014). Their traces in the fMRI signal are also uniformly postulated to reflect the increased cerebral blood flow and eventual dilution of deoxy-hemoglobin (Hgb) in the postcapillary part of vasculature, with additional effect of local blood volume increase (Kim & Ress, 2016).

In efforts to improve the efficiency of fMRI, studies have revealed various systemic physiological components in BOLD signal fluctuations. Physiological parameters, such as cardiac pulsation (Chang *et al.*, 2009), blood pressure, and end-tidal CO_2 (Wise *et al.*, 2004; Murphy *et al.*, 2013), are considered artifact sources. The contamination is expected to be emphasized in resting-state fMRI (rs-fMRI), where signals are evaluated without trial averaging (Winder *et al.*, 2017). However, discrimination between neuronal and non-neuronal components has been a major challenge due to the lack of validation techniques with comparable spatial and temporal precisions to those of fMRI. Another source of difficulty is the fact that many neural and non-neural parameters are intercorrelated in this low-frequency range (Murphy *et al.*, 2013).

A focus of recent studies exploring this matter is the spontaneous BOLD low-frequency oscillation (LFO, < 0.1 Hz) possibly encompassing multiple artifact sources (Zhu *et al.*, 2015; Tong *et al.*, 2017). One well-known sLFO source would be the respiratory volume fluctuation involving a chemoreflex loop (Birn *et al.*, 2008). An sLFO in systemic blood pressure, known as the Traube–Hering–Mayer wave, has been shown to originate from another autonomic loop (Guyton & Harris, 1951; Julien, 2006). Associated sLFOs in blood flow and velocity have been found (Killip, 1962; Fagrell *et al.*, 1977), and, later, transcranial Doppler ultrasonography and optical methods confirmed their traces within the brain (Giller *et al.*, 1999; Obrig *et al.*, 2000). This optically detected sLFO was found in

both oxy- and deoxy-hemoglobin (Hb) with an interesting phase difference exclusively observed in the brain (Rayshubskiy *et al.*, 2014; Tgavalekos *et al.*, 2016). sLFO was found even in electroencephalographic recordings, for which arterial vasomotion was suggested as the origin (Nikulin *et al.*, 2014), although it is unclear how the vasomotion accounts for the fMRI signal mainly from the capillary bed.

As mentioned above, Hb-sLFO is postulated to be of systemic origin (Katura *et al.*, 2006; Tian *et al.*, 2011; Sassaroli *et al.*, 2012). Hence it was not surprising to find a correlation between the global fMRI signal and extra-cerebral signals (NIRS or MRI), but the constant time shift across body/brain parts was unexpected (Anderson *et al.*, 2011; Tong *et al.*, 2012). The demonstration of the similarity between the low-frequency phase map and perfusion MRI in healthy participants was a milestone in this direction, by presenting the perfusion time lag embedded in the BOLD signal (Tong *et al.*, 2017). The resilient nature of the lag map against the fMRI task condition was shown, further supporting its non-neuronal origin (Aso *et al.*, 2017*a*). In parallel, a number of clinical studies have established the phase delays as a marker of cerebrovascular disorders (Amemiya *et al.*, 2013; Lv *et al.*, 2013; Christen *et al.*, 2015; Ni *et al.*, 2017; Nishida *et al.*, 2018; Khalil *et al.*, 2018). Gross vascular anatomy has been detected consistently in these studies, replicating the results from respiratory challenges (Chang & Glover, 2009*a*; Blockley *et al.*, 2011), which importantly suggests an equivalence between the sLFO and manipulated circulatory turbulences. Apart from patient data, a recent study involving healthy participants revealed changes in venous drainage pattern with normal aging (Satow *et al.*, 2017). A body of evidence thus empirically supports the biological significance of the low-frequency lag structure and its underlying principles.

The current analytical model of the BOLD lag structure assumes the presence of this signal variation from the very early stages of cerebral perfusion (Tong *et al.*, 2018)(**Fig. 1A**). Such synchronized variation should naturally affect the global mean signal and the model is hence related to the unresolved fMRI global signal problem (Liu *et al.*, 2017; Power *et al.*, 2017). This view is not only compatible with the occasional favorable effect of global signal regression (GSR) in task fMRI (Aguirre *et al.*, 1998) but has led some scientists to propose the removal of the lag structure as an approach for noise elimination (Erdoğan *et al.*, 2016; Amemiya *et al.*, 2016; Byrge & Kennedy, 2018). Under this model, the elimination of the lag structure can be viewed as an optimized GSR (of the low-frequency component) for each voxel group. Conversely, with the presence of the BOLD lag structure, a simple GSR should retain a residual correlation between in-phase voxels that confounds fMRI analyses (Taylor Webb *et al.*, 2013; Erdoğan *et al.*, 2016).

The fundamental and critical question remaining is the mechanism by which sLFO (or respiratory maneuvers) creates the BOLD lag structure. The BOLD response to neural activity via NVC is a well-documented passive process, involving the expansion of the intravascular compartment (Herman *et al.*, 2009). A typical model of the BOLD signal change is described as follows (Hoge *et al.*, 1999):

$$\frac{\Delta BOLD}{BOLD_0} = M\left(1 - \left(\frac{CMRO_2}{CMRO_2|_0}\right)^{\beta}\left(\frac{CBV}{CBV_0}\right)\left(\frac{CBF}{CBF_0}\right)^{-\beta}\right) \qquad [1],$$

where $CMRO_2$ stands for the cerebral metabolic rate of oxygen in a voxel, CBV/CBF for cerebral blood volume and flow, respectively. Beta is an exponent of the power-law describing the relationship between T2* and deoxygenated Hb (deoxy-Hb) amount that only depends on $CMRO_2$ and CBF in a reciprocal manner, under the assumption of negligible inflow of deoxy-Hb. M is the factor for the BOLD susceptibility effect defined as:

$$M \equiv TE \cdot B_0 \cdot CBV_0 \cdot [dHb]_{V0}^{\beta} \qquad [2],$$

where B_0 is the main magnetic field strength. Triggered by vasodilation of the arteriole, this effect is diminished by an inflow of fresh blood, which increases the MR signal. This baseline BOLD effect has been modelled in the formula for the off-resonance frequency shift as follows (Yablonskiy & Haacke, 1994; An & Lin, 2002):

$$\delta\omega = \gamma \cdot \frac{4}{3} \cdot \pi \cdot \Delta\chi_0 \cdot Hct \cdot OEF \cdot B_0 \qquad [3],$$

where γ is the gyromagnetic ratio (42.58 MHz/T), $\Delta\chi_0$ is the susceptibility difference between the fully oxygenated and fully deoxygenated blood, and Hct is the hematocrit (volume fraction of erythrocytes to the blood volume, typically around 40%). The oxygen extraction fraction (OEF) represents the only source of deoxy-Hb, again, under the assumption of 100% oxygen saturation (SaO_2) in the inflow. Variation of this base susceptibility can actually occur due to the local Hct and SaO_2 changes and, in fact, has been shown to cause intersession variabilities (Cohen *et al.*, 2002; Tuunanen & Kauppinen, 2006), but within-session fluctuations have rarely been considered (Thomas *et al.*, 2000). For example, even at a constant Hb density and oxygen partial pressure, CO_2 fluctuation, a driving factor of vasomotion, alone can modify SaO_2 through pH changes (Collins et al., 2015a). Although the assumption of constant base deoxy-Hb concentration may be sufficient for modeling its dilution by NVC (Ogawa *et al.*, 1998), other effects might not be negligible in non-neuronal fluctuations (**Fig. 1b**).

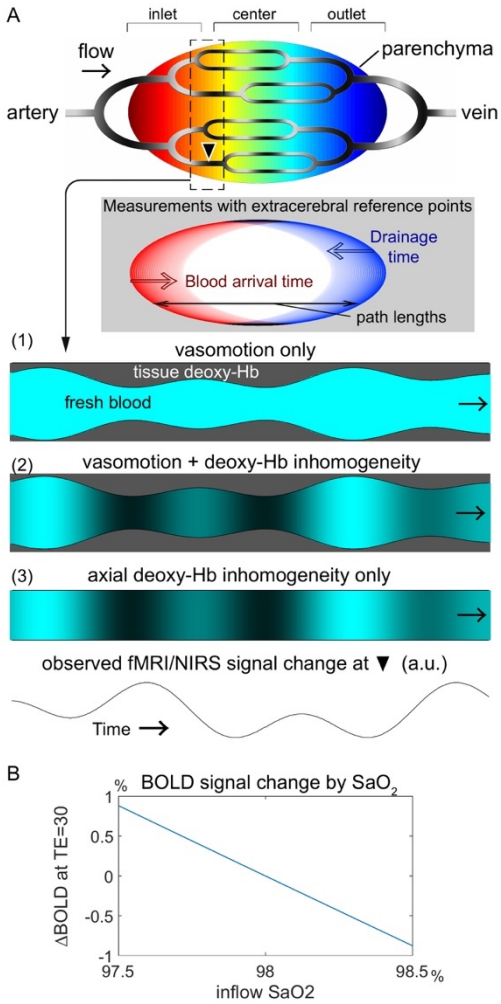

Fig. 1. Working model of the BOLD lag mapping. *A*, Schematic of the cerebral vascular tree presenting possible physiological models that account for the fMRI and NIRS observations. Each brain voxel has its lag (phase) of the spontaneous low frequency oscillation (sLFO) relative to the reference point, depicted in warm and cool colors. The inlet, center and outlet parts of the vasculature are determined purely by the temporal relationship and not by vessel types; all signals are supposed to originate from the capillary bed. Another schematic is inserted to illustrate the effect of the reference point selection in relation to the vascular path length, which accounts for the disagreement with other blood-tracking techniques. Below are shown three models with different physiological signal sources that are moving along the vasculature. While this axial inhomogeneity of the deoxy-hemoglobin (Hb) density may be linked with vasomotion (1), it can persist in the absence of vasomotion and flowmotion (2,3). The moving axial inhomogeneity would create a similar temporal profile with varying phase across regions. *B*, Dependence of the BOLD signal on inflow oxygen saturation (SaO2), a major determinant of deoxy-Hb concentration, at 3 T, TE = 30 ms. All other parameters were maintained constant at physiological values: oxygen extraction fraction = 45%, tissue blood volume fraction = 3%, and hematocrit = 40% (see Eqs. [1] and [2]).

In this exploratory study, we conducted three investigations to further advance our knowledge on the BOLD lag structure and its underlying physiology. We first evaluated if changes in blood transit velocity are embedded in the BOLD low-frequency phase to confirm its behavior as a virtual tracer [a preliminary analysis of these data was presented previously as a poster (Aso *et al.*, 2017*b*)]. Next, we investigated the effect of eliminating the lag structure from task-based fMRI, which has not been tested yet. Finally, we used multi-echo imaging to assess the components of the BOLD signal that determine the lag structure. One of the recent approaches toward fMRI denoising has focused on S_0 fluctuation (signal at echo time = 0, which is the baseline MR signal from the fluid compartments), as it is weakly associated with neural activity (Posse *et al.*, 1999; Wu *et al.*, 2012; Kundu *et al.*, 2012; Yen *et al.*, 2017). In contrast, the total-Hb sLFO, detected by NIRS, is interpreted as a local CBV change under the assumption of a constant Hct, which should also affect the non-BOLD component via changes in plasma volume and inflow (Rostrup *et al.*, 2005). Again, the T2* and S_0 components may contribute in a different manner than NVC to the BOLD lag structure that have been overlooked in studies based on trial averaging. From the influences of three different fMRI task paradigms, including a simple reaction-time visuomotor task, a short breath-holding task, and a hyperventilation task on the neural and non-neural components of the fMRI signal, we sought further validation of our hypothetical model of the BOLD lag structure.

2 Materials and methods

2.1 Subjects and experimental procedures

Twenty-one healthy subjects (eight women, 19–26 years of age) participated in Experiment 1; one subject was excluded from the analysis because of abrupt head motion, which prevented BOLD lag mapping (see Data processing). The remaining 20 participants performed the sparse visuomotor and 10-s breath-holding tasks, but the hyperventilation task was only performed by 18 participants, as it was introduced after the first two participants had concluded their participation. Another 21 participants were recruited for Experiment 2, involving multi-echo acquisition, all of whom performed the above three tasks but with an 18-s version of the breath-holding task. To avoid vigilance level fluctuations, all MRI sessions were scheduled in the morning and the participants were encouraged to sleep well the previous night.

The protocol for this study was approved by the internal ethics review board of Kyoto university. The subjects provided written informed consent in advance, according to the Declaration of Helsinki, for the analysis of anonymized MRI scans and simultaneously acquired physiological data.

2.2 Image acquisition

A Tim-Trio 3-Tesla scanner (Siemens, Erlangen, Germany) with a 32-channel phased-array head coil was used for MRI acquisition. For Experiment 1, T2*-weighted echo-planar images were acquired using multiband gradient-echo echo-planar imaging (EPI) (Feinberg *et al.*, 2010) with the following

parameters to cover the entire cerebrum: 64 × 64 pixels, interleaved 35 slices, 192-mm field of view (FOV), 3.5-mm slice thickness, repetition time (TR)/echo time (TE) = 500/35 ms, flip angle = 40°, and multiband factor of five. Three 9-min runs (1,080 volumes) were acquired for each of the three task conditions. The same pulse sequence program was used in Experiment 2 but with multi-echo settings: TE1 = 7.76 ms and TE2 = 25.82 ms for the first six subjects and TE1 = 11.2 ms and TE2 = 32.78 ms for the remaining 15 subjects. A smaller multiband factor of two was selected to allow for the short TE in combination with a parallel imaging using GRAPPA. Other acquisition parameters were: TR = 1,300 ms, flip angle = 65°; interleaved 36 slices, FOV = 256 × 192 mm^2, 64 × 48 matrix, 3.5-mm slice thickness. Three 7-min (323 TRs) runs were acquired. Seven subjects in Experiment 2 underwent two additional runs with a shorter TR of 700 ms and a flip angle of 45° to examine the sensitivity of the respiration-related signal component to inflow modulation. At the end of every experimental session, a 3D MPRAGE T1-weighted image was acquired for obtaining anatomical information (Aso *et al.*, 2017*a*). A dual-echo gradient-echo dataset for B0 field mapping was also acquired after the BOLD scan in the same orientation.

2.3 Task conditions

Throughout the experimental session, task instructions were presented via an LCD monitor inside the scanner room, viewed through a mirror. Beat-to-beat fluctuations in the mean arterial pressure and heart rate were obtained via a non-invasive MR-compatible device (Caretaker, BIOPAC Systems, Inc., Goleta, CA, USA). Careful instructions were provided to the participants on how to avoid motion, especially during the respiratory challenges.

2.3.1 Sparse visuomotor task

A simple visuomotor task with a varying intertrial interval of 6 to 24 s was performed during the first run. Subjects were instructed to press a button with their right index finger as soon as the computer screen changed from “Please hold still” to “Press the button.” The screen returned to “Please hold still” at the button press or after 3 s, if the participant had not pressed the button.

2.3.2 Breath-holding task

To minimize head motion induced by the tasks, the two respiratory challenges were adapted to be less strenuous than in earlier studies. In Experiment 1, the breath-holding task was cued by a “Hold your breath” instruction on the screen, at which point the subjects were asked to immediately hold their breath, irrespective of the respiration phase. The holding periods lasted for 10 s and were separated by 90-s intervals. This short duration was selected to minimize strain that can cause body movements, while evoking a detectable autoregulatory response (Murphy *et al.*, 2011). In Experiment 2, a longer holding period of 18 s after a brief inhalation for 2 s was used to evoke a more pronounced vasodilation.

2.3.3 Hyperventilation task

The hyperventilation task involved paced breathing at 1/5 Hz for 25 s, separated by a 30-s rest. Each 5-s cycle began with the screen presenting "Please inhale" for 1.5 s, followed by "Please exhale slowly," lasting 3.5 s. Subjects were instructed to breathe as deeply as possible, while avoiding head movement. A short inspiration period was selected to suppress motion by minimizing movements in the thoracic cage and spine.

2.4 Data processing

For image processing, SPM12 (Wellcome Department of Cognitive Neurology, London, United Kingdom) and FSL5 (FMRIB Software Library, www.fmrib.ox.ac.uk/fsl) (Smith *et al.*, 2004) were used in combination with in-house MATLAB scripts. Off-resonance geometric distortions in the EPI data were corrected using FUGUE/FSL with B0 field maps. After inter-scan slice-timing correction, head motion was compensated by 3D motion correction and data repair (Mazaika *et al.*, 2009). The repairing procedure aimed to remove motion-related signal dropout and involved searching for time points satisfying two stringent criteria: (1) global signal change between consecutive volumes exceeding 1% and (2) head displacement exceeding a Euclidian distance of ±1 mm or ±1° rotation per TR. The affected time points were replaced with linearly interpolated values, but this procedure was required in only six of the 41 participants. The data were further cleaned by regressing out 24 head motion-related parameters. Unlike in previous studies, the six rigid-body parameter timeseries were not directly used because of the possible contamination of the motion parameters with the global signal when the subjects were immobile (Freire & Mangin, 2001). We used the first temporal derivatives of the motion parameters, their shifted versions by 1 TR, and the squares of those 12 timeseries (Satterthwaite *et al.*, 2013). Images were spatially normalized to the template space using the T1-weighted anatomical image and resliced to a 4-mm isotropic voxel size to achieve a high voxel temporal signal-to-noise ratio.

2.4.1 Lag mapping

A recursive technique was used (Aso *et al.*, 2017*a*) after temporal bandpass filtering at 0.008–0.07 Hz to ensure that the phase was uniquely determined within the cross-correlation range. Whereas lag was tracked up to 7 s for most analyses, it was limited to 4 s in both directions, upstream and downstream, for the calculation of the relative BOLD transit time (rBTT, see below). This shorter tracking range allowed a higher cutoff frequency (0.12 Hz) to preserve the high-frequency component in the velocity change profiles.

The global mean signal was used to select the initial seed that defined the reference phase (lag = 0). First, voxels presenting a cross-correlogram peak at 0 with the global signal were determined. The time course averaged over this set of voxels served as the initial reference. In each step of the recursive procedure towards up- and downstream, a cross-correlogram was calculated between the timeseries obtained from the previous seed voxels and every undetermined voxel to find a set of

voxels with a peak at ± 0.5 s, which then served as the new seed. This tracking part retained some voxels without any lag values because cross-correlogram peaks < 0.3 were not used (Tong et al., 2017). These voxels were later filled one by one with average phases from voxels with similar time courses at correlation coefficients > 0.3. There were single isolated holes even after this procedure, which were filled by linear interpolation, using the six neighbors. There is a concern that this threshold of correlation coefficient is too low to claim significant correlation. However, the recursive tracking involves finding the cross-correlogram peak precisely at ±0.5 s, which conveys different information from its height. Besides, a majority of earlier works, empirically supporting biological significance of this phenomenon, involved no thresholding. When the threshold correlation-coefficient was increased to 0.6, most brain voxels required the hole-filling procedure, but we still obtained similar lag maps (by between-voxel intra-class correlation ICC(2,1) > 0.4) in 16 out of 20 subjects.

2.4.2 fMRI analysis on "cleaned" BOLD datasets

Individual BOLD data from Experiment 1, after the above pre-processing steps including the motion parameter regression, served as the reference or "raw" dataset. GSR with low-pass filtered global signal, normal GSR, global scaling implemented in SPM12, and removal of the perfusion lag structure ("deperfusioning") were compared with the raw dataset.

The GSR involves regression by the global signal and extracting the residuals in each voxel. In deperfusioning, instead of the uniform regressor, a corresponding timeseries was used for each voxel group by the lag value ("dynamic" GSR) (Erdoğan *et al.*, 2016). For global scaling, the raw dataset was entered into the same SPM pipeline, except for the option of internally dividing each volume by its global mean signal instead of the constant session mean. The normal GSR and global scaling thus affected all frequency ranges, whereas the filtered GSR and deperfusioning removed only the low-frequency components.

Random effects analysis (Friston *et al.*, 2002) was used to evaluate the effect of these procedures on the fMRI results from the standard analysis framework. For the visuomotor task, the neural response to each trial was modeled as an event of 0.5-s duration. For the hyperventilation condition, a boxcar with 25-s duration modeled the activation related to volitional respiratory control. Similarly, both the onset and offset timing of breath holding were used to model the time-locked neural activity. The canonical hemodynamic response function was convolved to the model timeseries to create the regressors of interest. All activation maps were thresholded at $p = 0.05$ after correcting for multiple comparisons, using family-wise error across the whole brain (Poline *et al.*, 1997).

2.4.3 Relative BOLD transit time

Fig. 3A illustrates the method. This analysis was performed on data from Experiment 1, acquired at a short TR of 0.5 s. The lag structure consisted of a lag map and the set of timeseries averaged over

291 the voxels with the same phase. This structure represents the propagation of the sLFO phase along
292 the vessels. The phase is expected to move across adjacent regions of the vascular tree every 0.5 s,
293 the lag tracking step, on average. However, if there is variation in propagation velocity, there would
294 be deviation of the instantaneous phase difference from 0.5. Here, the phase difference is supposed
295 to reflect the time the blood requires to cross the boundary between the neighboring voxel groups.

296 Based on this supposition, the phase difference fluctuation was calculated from each of the 16 pairs
297 of seeds corresponding to lags of -4 to +4 s at 0.5-s intervals. Because of the broad frequency range
298 of the fluctuations of interest, we chose smooth sliding window algorithm (window length = 30 s,
299 Kaiser window with a parameter beta of 4) instead of analytic methods (e.g., Hilbert transform). The
300 region timeseries were resampled to a 0.02-s resolution to capture minute phase difference
301 fluctuation (4%) from 0.5 s. Instantaneous phase differences from each pair of seeds were averaged
302 over respiratory task events and divided by 0.5 to obtain the time course of the rBTT. The rBTTs
303 from the 16 pairs of neighboring regions were then averaged to obtain the regional or global rBTT.
304 According to this model, the inverse of the rBTT corresponded to the instantaneous velocity
305 (relative to the baseline average velocity), as the rBTT should reflect the average time the required
306 to traverse fixed distances.

307 **2.4.4 Multi-echo combination**

308 For Experiment 2, involving multi-echo acquisition, S_0 and T2* datasets were created by a simple
309 estimation used in earlier works (Posse *et al.*, 1999; Yen *et al.*, 2017). We assumed a single
310 compartment monoexponential decay of the MR signal as follows:

311

312 $$\boldsymbol{S(TE) = S_0\ exp(-TE/T_2{}^*)} \qquad [4],$$

313

314 where T2* and S_0 were calculated for each TR as follows (Kundu et al., 2012; Posse et al., 1999):

315

316 $$\boldsymbol{T_2{}^* = (TE2 - TE1)/\ln\,(S_1/S_2)} \qquad [5] \text{ and}$$

317

318 $$\boldsymbol{S_0 = S_1{}^{TE2/(TE2-TE1)}/S_2{}^{TE1/(TE2-TE1)}} \qquad [6],$$

319

320 where S_1 and S_2 are the acquired signals at TE1 and TE2, respectively. Negative values or T2*
321 exceeding 100 ms were considered as noise and were ignored. All four datasets (S_0, S_1, S_2 or BOLD,
322 and T2*) were entered into the same analysis pipeline used for Experiment 1 but taking the
323 different TR of 1.3 s into account. The following analyses were performed on a resampled time
324 course at a TR of 0.5 s.

The interaction between the signal component and vascular anatomy was examined by extracting the signal timeseries from the inlet, center, and outlet parts of the vascular tree, based on the individual lag map created from the BOLD (i.e., at TE2) dataset. By exploiting the longer lag tracking range (± 7 s) than the one used in the rBTT analysis in Experiment 1, the center region in this analysis covered a wider range (± 2.5 s). Using the JMP12 Software (SAS Institute, Cary, NC), the magnitude and phase of the regional signals were analyzed by repeated-measures ANOVA followed by post hoc analysis, using Tukey's honestly significant difference (HSD) test. Statistical significance was assumed for $p < 0.05$. Additional analyses were performed to examine the origins of the signal components, including a region-of-interest analysis and an SPM analysis of respiration phase-related small S_0 fluctuation.

3 Results

The average root mean square of head motion measured as the framewise displacement, i.e., the shift in the position of the brain in one volume compared to the previous volume, was 0.039 ± 0.007 mm (mean ± standard deviation over subject) for Experiment 1, with a maximum displacement of 0.37 ± 0.18 mm, and 0.034 ± 0.015 mm for Experiment 2, with a maximum of 0.24 ± 0.12 mm (Van Dijk et al., 2012).

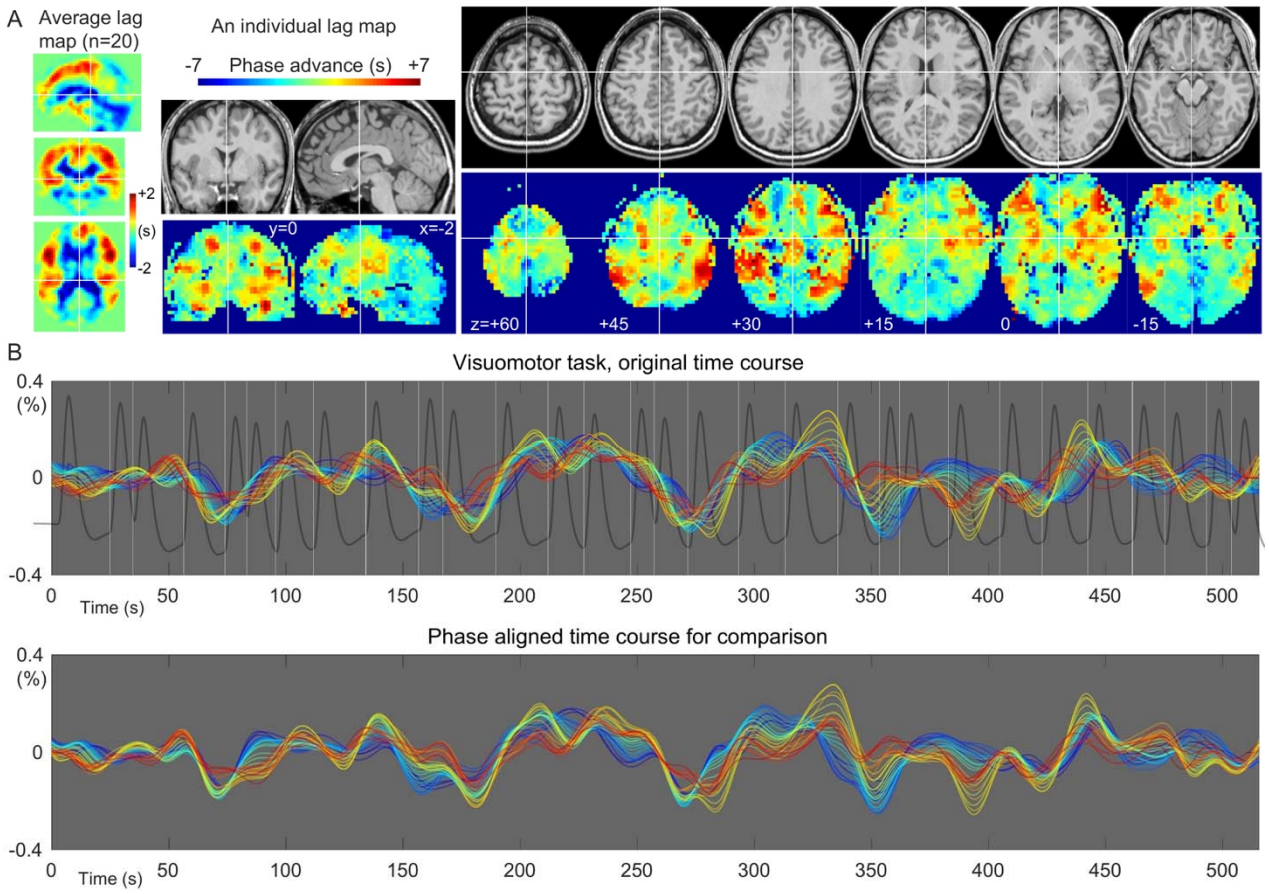

Fig. 2. Representative spatial and temporal profiles of the BOLD lag structure. (A) Lag map created by tracking the BOLD low-frequency oscillation (LFO) phase up to 7 s toward both up- and downstream. Group average map shows the gross vascular anatomy with the early phase (positive values) distributed in the middle cerebral artery territories. The individual map provides more detailed information. (B) Seed time courses updated at each step (0.5 s) of the recursive lag tracking procedure, representing the temporal aspect of the lag structure. The warm-colored traces with advanced phase originate from the voxels with the same colors in the lag map, corresponding to the inlet or arterial side of the vasculature. A gradual change in the temporal profile is noted on top of the slow component, which is stable across regions. The white vertical lines indicate the timing of the visuomotor task, whose NVC was modeled by the hemodynamic response function (dark gray trace). The detected LFO was poorly correlated with the task-related fluctuation of neuronal origin (see main text).

Fig. 2A shows the average and an individual BOLD lag map during the sparse visuomotor task. Warm colors indicate a positive travel time from those voxels to the phase of the global LFO, signifying that the voxels are considered "upstream." Most brain voxels fell into the -4 to +4 s range (mean ± SD, 93.8 ± 2.9%). The recursively defined seed time courses are shown in **Fig. 2B** with warm colors indicating averaged timeseries from the upstream voxels. This time course of the lag structure was poorly correlated with the visuomotor task (white vertical lines) or the evoked NVC response (trace in dark gray), supporting non-neuronal origin of the sLFO. This was confirmed by the correlation coefficient between the global mean signal and the modeled response that was not significantly different from zero (0.0265 ± 0.140, mean and SD over 20 participants), although still slightly positive in some subjects and its regression affected the activation maps (see section 3.2). In addition to the constant phase shift across regions, the lag structure time courses presented minute fluctuations of the phase difference (i.e., the temporal relationship between the lines) over time.

3.1 Flow velocity information in the instantaneous phase

A transient change in propagation velocity of the low-frequency phase, obtained as the inverse of the global rBTT, was found in response to the respiratory challenges. **Fig. 3B** shows the stacked histograms of distribution of instantaneous phase difference measured by the moving window analysis. This instantaneous phase difference (in s) is interpreted as the time the blood required to move over a unit distance that requires 0.5 s on average. The time courses are presented in **Fig. 3C**. After approximately 10 s of delay, increase and decrease of the BOLD signal was found during breath holding and hyperventilation, respectively (arrows). This delay in the autoregulatory BOLD response is consistent with earlier work (Murphy *et al.*, 2011).

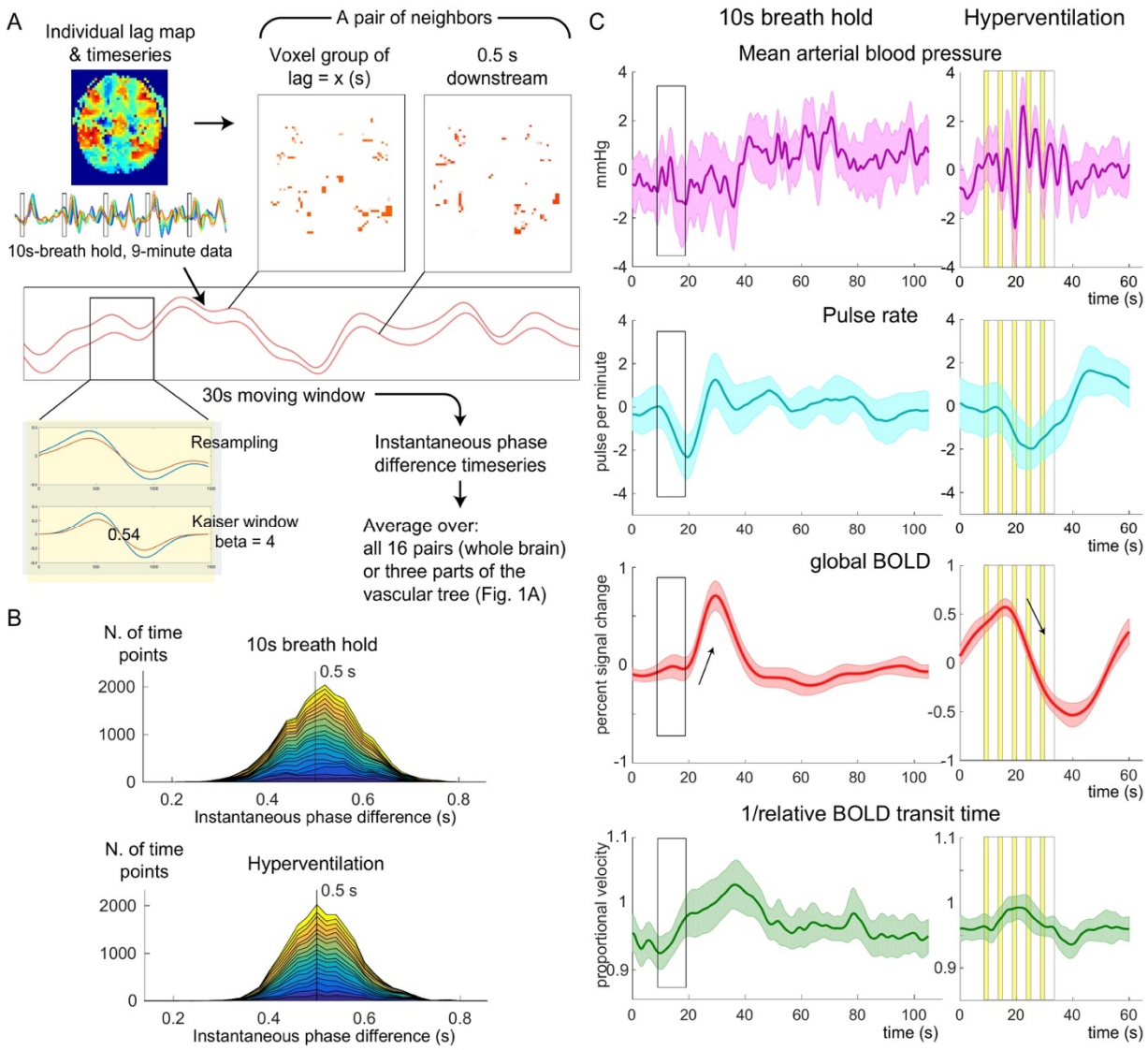

Fig. 3. Measurement of relative bold transit time (rBTT). (A) Schematic illustration of the analysis. For each pair of voxel groups representing neighboring regions of the vascular tree, the two average timeseries were fed into a moving window analysis of instantaneous phase difference. (B) Time point histograms of the instantaneous phase difference averaged over 16 pairs of neighboring regions in the lag structure. Twenty subjects are stacked. Deviation of the phase difference from 0.5 s reflects a fluctuation of the flow velocity, although the slight shift of the peak is observed in the breath hold data presumably due to the effect of windowing. (C) Response to the respiratory challenges of the physiological recordings, the raw BOLD signal, and inverse of the rBTT that can be interpreted as relative velocity. Thin arrows indicate the autoregulatory response of the raw BOLD signal. The five cycles of volitional breathing for hyperventilation are indicated with yellow bands representing the inspiration phase. Shaded areas indicate the 95% confidence interval of the mean across subjects.

The temporal profile of the instantaneous velocity (green curves) was roughly in phase with the global BOLD response but had different onset and peak timings, indicating the different physiological bases. To evaluate the relationship of this phenomenon with the vascular structure,

392 the inlet, center, and outlet regions were separately analyzed (**Fig. 4**). In both respiratory challenges,
393 there was a clear asymmetry over the vasculature, with pronounced velocity responses in the inlet
394 region. Despite similar BOLD response profiles, the velocity response was not clearly found in the
395 outlet region.

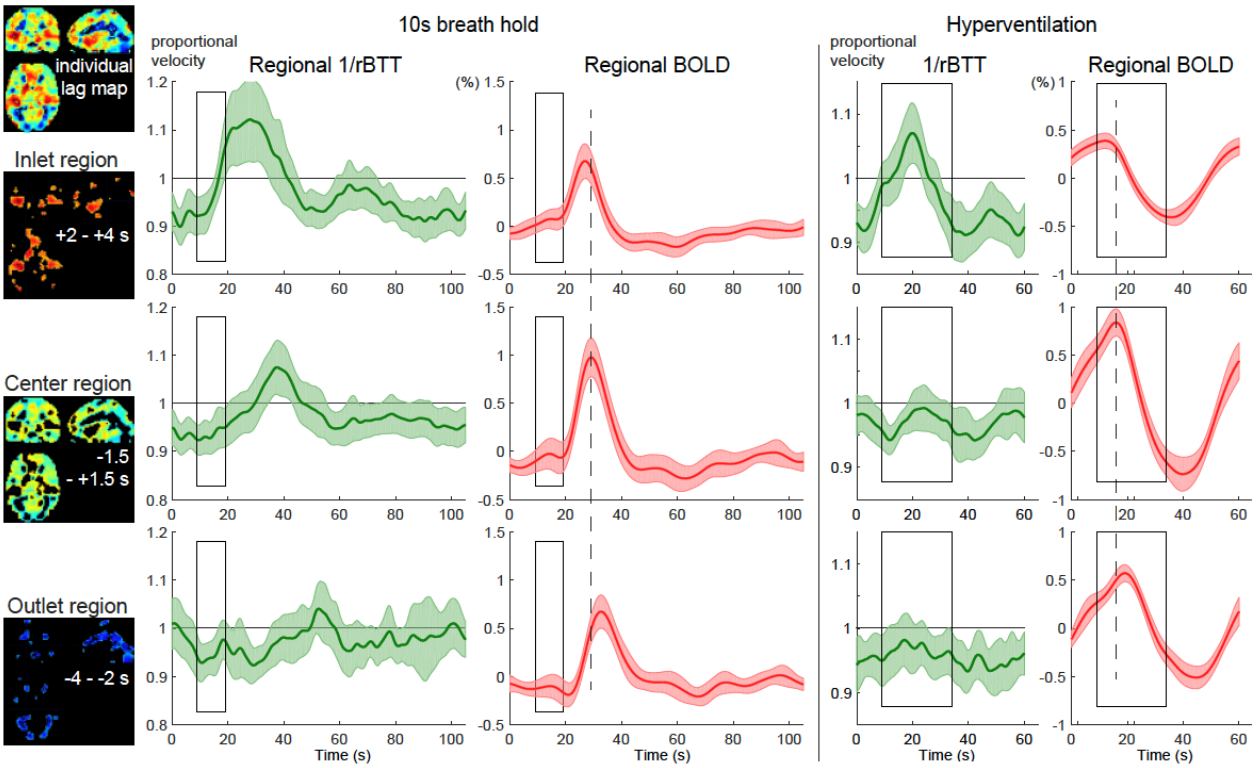

396

397 **Fig. 4.** Autoregulatory responses to respiratory challenges in the three vascular regions, using
398 the same conventions as in **Fig. 3**. The inlet (arterial side), center, and outlet (venous side) of the
399 parenchymal vasculature were defined for each subject, using the lag map created from the
400 session data per se. The relative changes in propagation velocity were detected as the inverse of
401 instantaneous transit time deviation from 0.5 s (rBTT), since the lag mapping was performed at
402 0.5-s steps. The BOLD signal time courses present different peak latencies for the three regions
403 (broken lines are aligned to the center region peak), directly reflecting the lag structure, but with
404 similar profiles, ruling out its effects on the rBTT measurement. Shaded regions represent the
405 95% confidence intervals (N = 20).

406

407 **3.2 Effect of deperfusioning on the detection of NVC**

408 Removal of the whole lag structure exhibited unique effects on the fMRI analysis. While the mean
409 and standard deviation images from the individual activation maps showed similar spatial
410 distribution, all procedures reduced the sensitivity compared to the Raw dataset where only the
411 motion-related variances were removed (**Fig. 5**). However, after the deperfusioning procedure,
412 primary motor cortex activation was successfully detected by decreased interindividual variances

(black circles). The effect of these procedures was not uniform between the respiratory challenges (**Fig. 6**), but some interpretable clusters were selectively captured by the "deperfusioned" signals despite the reduced cluster number. For example, the so-called laryngeal motor cortices were detected at the onset and offset of the 10-s breath-holding (Kumar *et al.*, 2016). In the hyperventilation condition, bilateral recruitment of the putamen was noted. This is consistent with reports using optimized acquisition techniques (Dresel *et al.*, 2005; Pattinson *et al.*, 2009), supported by anatomical (Simonyan & Jürgens, 2003), as well as electrophysiological (Radna & MacLean, 1981) studies. A premotor peak found at coordinates [+56, 0, 40] was also very close to the reported activation site for volitional respiration (McKay *et al.*, 2008).

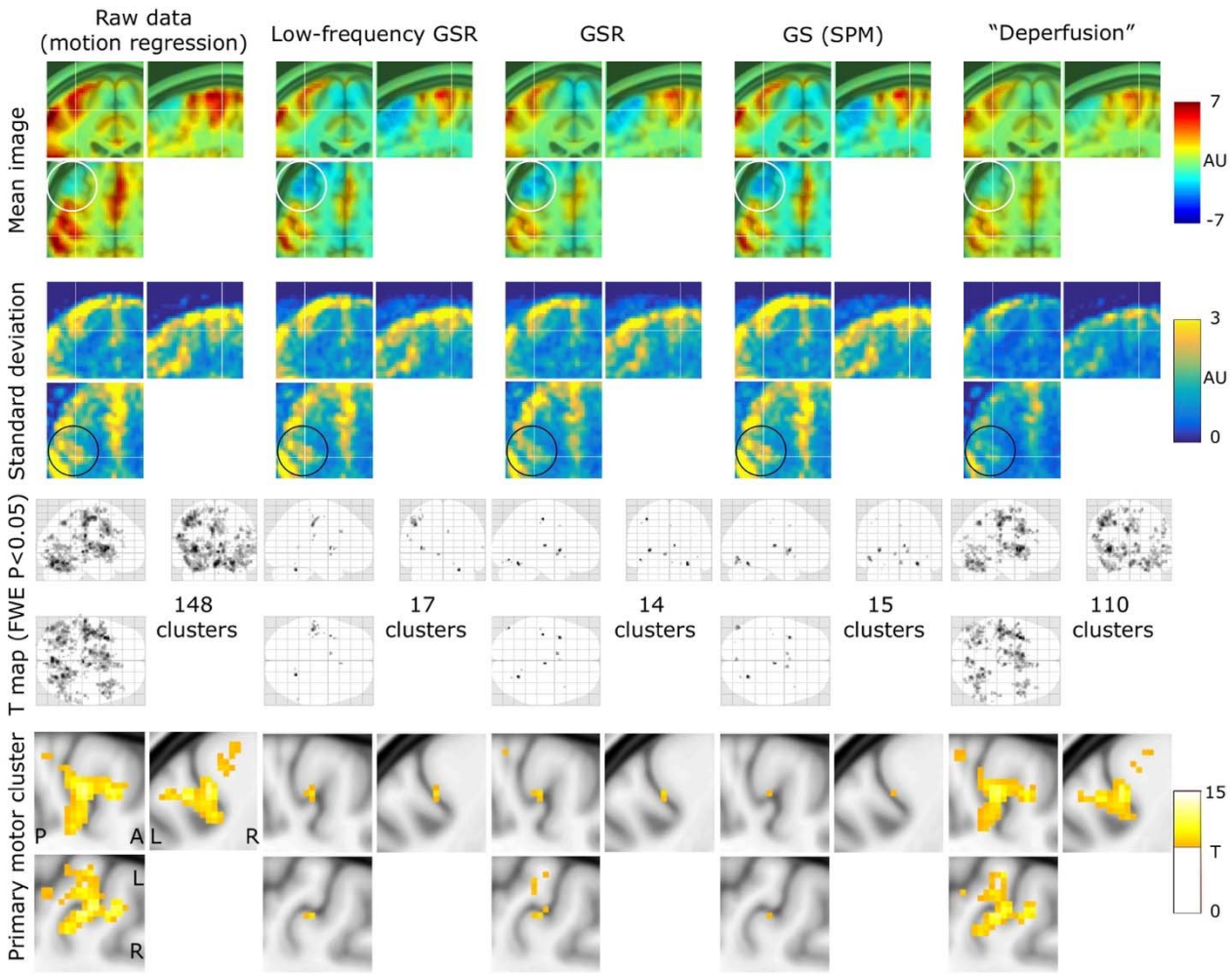

Fig. 5. Effect of the denoising procedures on the detection of neurovascular coupling during the visuomotor task. Mean and standard deviation maps from 20 individual activation maps (contrast images) illustrate the spurious negative responses by the global-signal based methods (white circle) and the reduced between-subject variation by the lag structure removal or deperfusioning (black circle). Activation maps were thresholded at p = 0.05, corrected for FWE of multiple comparisons over the entire brain, and zoomed in to show the "hand-knob" of the left primary sensorimotor cortex. FWE, family-wise error corrected.

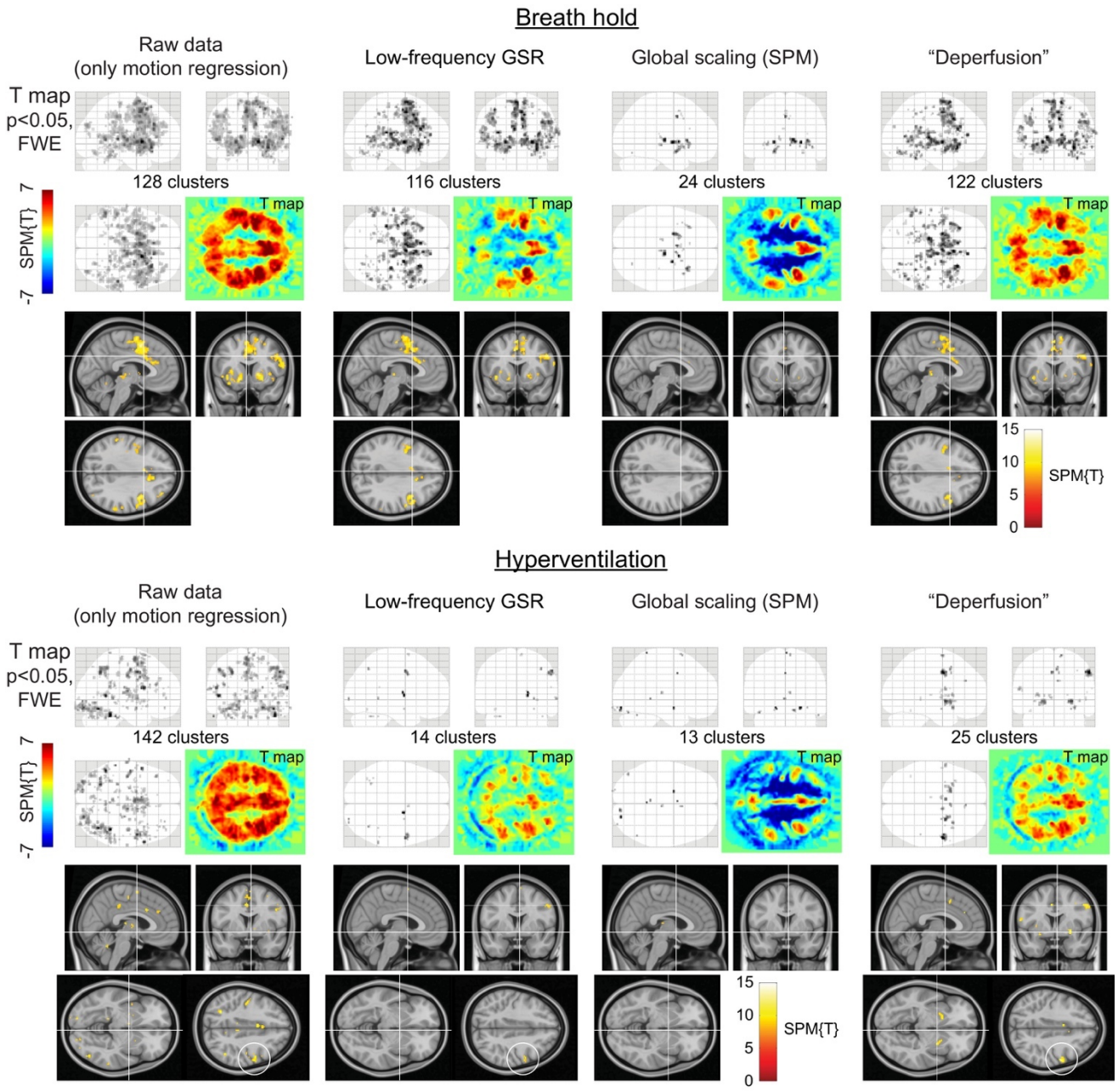

Fig. 6. SPM results of the respiratory challenges. Color panels show un-thresholded t map slices at the height of the laryngeal motor cortex (z = 35) (Kumar et al., 2016), revealing spurious negative responses (cool colors) after global signal removal but not after the deperfusioning procedure. In the hyperventilation condition, the "deperfusioned" data revealed clusters in the bilateral putamen and premotor cortex (white circle), consistently with the findings of earlier reports.

Voxel histograms from the group SPMs showed clear leftward shifts by the global signal removal, indicating spurious deactivations (**Fig. 7**). The correlation of the neuronal response with the global signal (or the extracted sLFO) was near zero, as described above, but it varied across subjects and

tended to be positive. This trace of NVC may have created the spurious deactivation after regression. Notably, this effect was very weak after deperfusioning across all three conditions (green plots), despite a large amount of variance removed by the procedure. This finding is in agreement with the results of earlier work on resting-state fMRI (Erdoğan *et al.*, 2016).

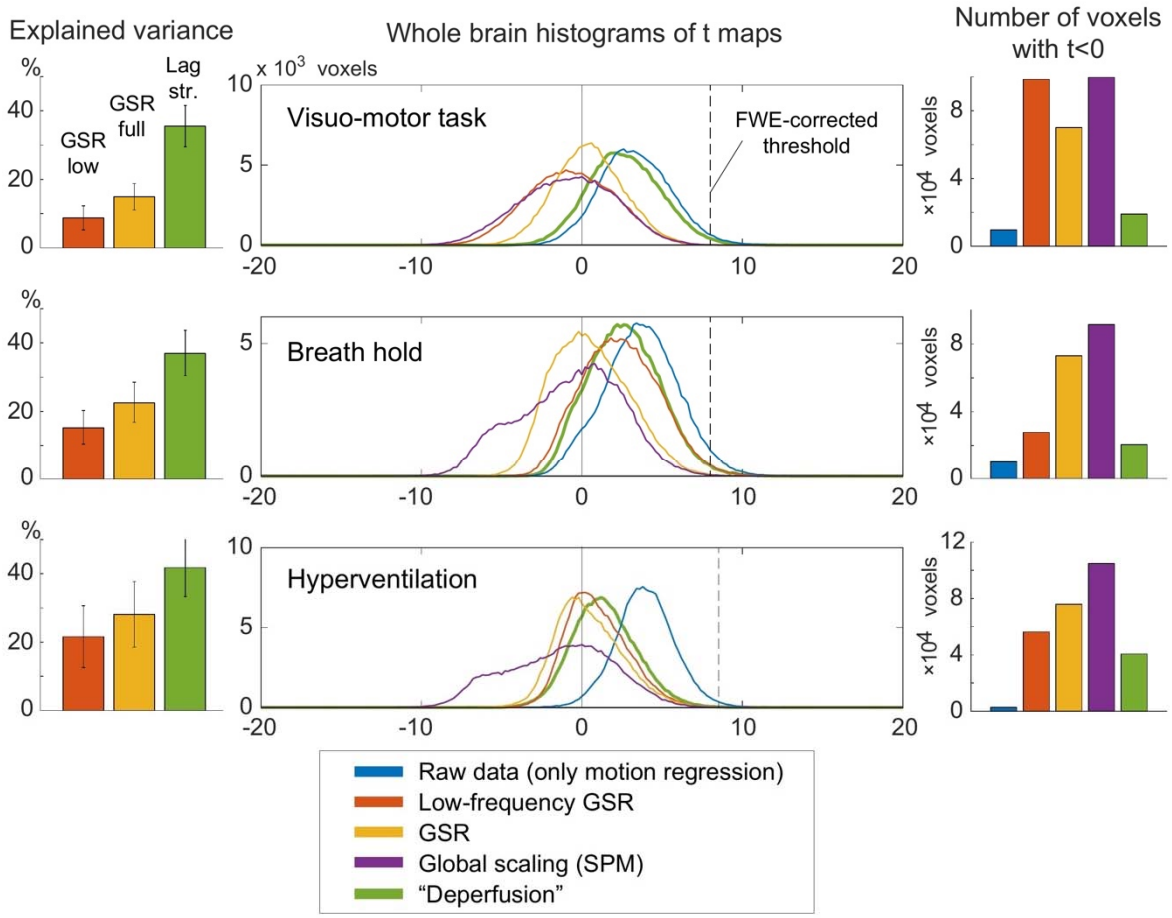

Fig. 7. Effect of preprocessing on group SPMs. Removal of the lag structure or deperfusioning resulted in greatest reduction of the signal variance under all three tasks (left panels). Nevertheless, the spurious negative task responses were attenuated in comparison to the removal of global fluctuation (middle and right panels). Error bars indicate the standard deviation. The vertical broken line in the histogram indicates the statistical height threshold of p = 0.05, corrected for multiple comparisons by family-wise error rate. GSR, global signal regression.

3.3 MR signal components of the lag structure

As depicted in **Figure 8**, the percent signal change of the sLFO, or the lag structure amplitude, revealed a clear T2*-dependence with a significant reduction of amplitude in the outlet, i.e., the venous side of gross vasculature (post hoc Tukey's HSD between T2* signals from the inlet and

outlet regions, following a repeated-measures ANOVA). This finding replicates a previous observation in the raw BOLD signal (Aso *et al.*, 2017*a*).

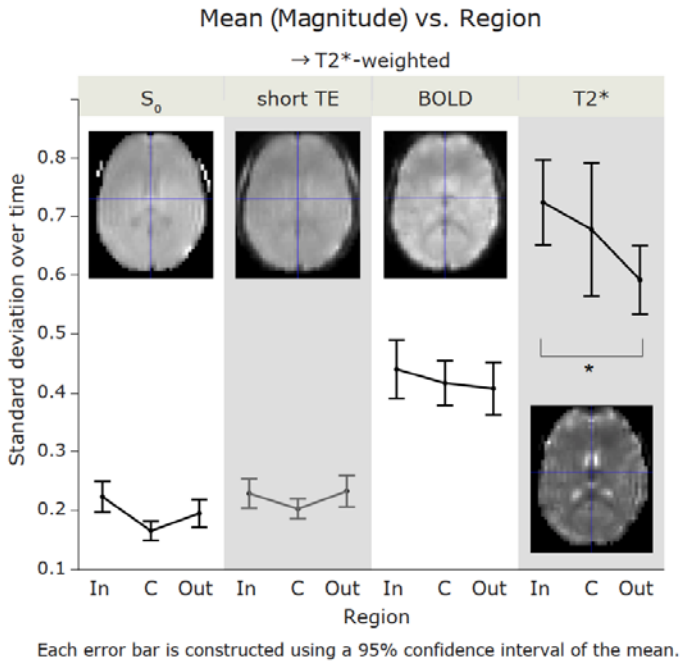

Fig. 8. Standard deviation of the percent signal change as a measure of sLFO magnitude. No main effect of vascular region was observed by repeated-measures ANOVA, but the T2* magnitude was significantly different between the inlet and outlet or arterial and venous sides ($p < 0.05$, Tukey HSD). The short-TE image was not included in the ANOVA to avoid data redundancy.

In lag maps from the three T2*-weighted images, we noted some effect of the respiratory challenges, but the gross cerebral vascular structure was preserved across tasks; the periventricular regions and major venous sinuses were uniformly found downstream (i.e., with negative arrival time) of the global signal phase, while the cortical territory of the middle cerebral arteries presented earlier arrival (**Fig. 9A**). Only the S_0 image presented a different lag structure, which was confirmed by the image similarity (**Fig. 9A**, right panels).

Temporal analysis of the signal components revealed significant main effects of both region [$F(2,532) = 16.877$, $p < 10^{-6}$] and T2* weighting [$F(2,532) = 280.786$, $p < 10^{-6}$] (**Supp. Fig. 1A**). The S_0 timeseries failed to show a correlation with the T2*-weighted signals, but the z-value in the inlet, i.e., the arterial side, differed significantly from other regions ($p < 0.05$, Tukey's HSD). A region effect was also found for phase relationships (**Supp. Fig. 1B**). Again, the main effects for both region [$F(2,532) = 27.548$, $p < 10^{-6}$] and T2* weighting [$F(2,532) = 44.679$, $p < 10^{-6}$], as well as their interaction [$F(4,532) = 24.902$, $p < 10^{-6}$], were significant. The phase of the TE1 signal, which is less T2*-weighted than is BOLD, gradually advanced, finally showing a phase lead in the outlet region, further supporting an interaction between the signal components and vascular regions. These signal

phase dissociations within regions are displayed in **Supp. Fig. 1C**. Significant differences among the three T2*-weighted signals were also found after the post-hoc test ($p < 0.05$). The signal-region interaction was evident in the signal response to the respiratory challenges shown in **Fig. 9B**. The traces contain higher frequency components, which were eliminated for lag mapping. In contrast to the changes in T2* responses for both phase and magnitude, the S_0 component was stable across vascular regions.

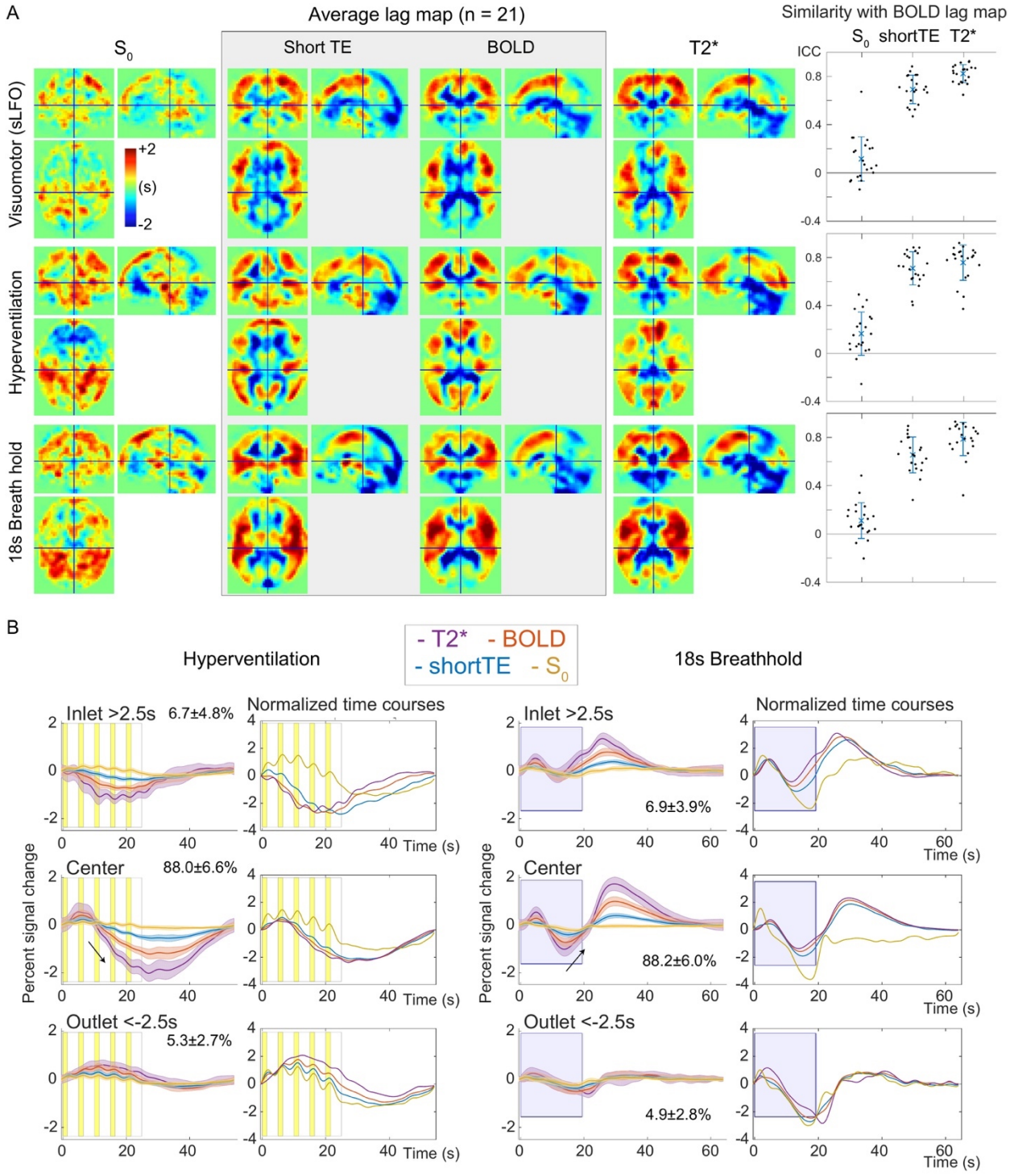

489 **Fig. 9.** Analysis of signal components and the lag structure. *A*, S_0 and T2* signals were
490 interpolated based on multi-echo acquisition at short and typical echo times for BOLD fMRI. The
491 lag map created from the S_0 image shows a unique structure but fails to reflect the arterial and
492 venous structures that are consistently found in the BOLD lag map. Using the T2*-weighted
493 signals, the lag map changes upon respiratory challenges, which should primarily reflect the
494 modification of the perfusion pattern; however, an interaction with the signal component is not
495 excluded. The right panels show intraclass correlation coefficients as a quantitative measure of
496 within-subject image similarity with the BOLD lag map, with error bars indicating 95%
497 confidence intervals. *B*, Temporal profiles from the three vascular regions indicate absence of
498 region effect in the S_0 signal, suggesting a globally uniform mechanism underlying the S_0
499 response.

500

501 To further investigate the signal origin, we extracted the response in the motor/premotor area
502 activation peak, where NVC was expected to dominate (**Supp. Fig. 2A**). For this analysis, the group
503 activation map from Experiment 1 was used to define the regions-of-interest in order to avoid bias.
504 We found high-frequency components dominating the S_0 responses in comparison to the responses
505 from larger regions shown in **Figure 9B**. During hyperventilation, it presented respiratory phase-
506 related fluctuations, with a signal decrease initiated by inhalation and followed by a positive
507 deflection during exhalation. The T2* signal also exhibited small fluctuations but with a different
508 phase, possibly dominated by the NVC component.

509 We conducted an additional analysis for this fast respiration-related non-BOLD component. The
510 spatial distribution of this response is shown in **Supp. Fig. 2B**. Interestingly, there was a clear
511 anterior-posterior segmentation of response polarity, with the posterior regions presenting the
512 opposite phase of this fast S_0 deflection by respiratory maneuver. Some additional symmetrical
513 structures were found in deep-brain regions, near the deep middle cerebral and inferior ventricular
514 veins, implying a unique vascular involvement. Importantly, this spatial pattern was not that of a
515 typical motion artifacts that can accompany volitional respiration in spite of the careful instruction.

516 Finally, **Supp. Fig. 2C** shows the data from a subset of participants, obtained using a different
517 TR/flip-angle setting to manipulate the inflow effect. The T2* response was smaller than that shown
518 in the panel **2A**, presumably due to the short TR. The different TR also contributed to the rich high-
519 frequency components by the fast sampling rate. The slow S_0 change was also diminished, but the
520 respiration-related fast component was relatively preserved suggesting absence of a strong inflow
521 effect.

522 **4 Discussion**

523 The principal findings of this study are summarized as follows. First, based on the instantaneous
524 phase difference within the BOLD lag structure, we observed a trace of blood flow velocity change

525 selectively in the inlet region of the vasculature. Next, the complete elimination of the lag structure
526 reduced interindividual variance and spurious deactivation, supporting our hypothesis that NVC
527 could be observed more specifically by this deperfusioning procedure. Finally, the lag structures in
528 the S_0 (or non-BOLD) component did not correlate with that from T2*, either spatially or temporally.
529 We also found a vascular region-dependent change in the T2* LFO, with a decreased amplitude in
530 the venous side, in contrast to the S_0 response that remained constant in both amplitude and phase.
531 The S_0 component exhibited a unique brain region-dependent response to the respiratory phase,
532 suggesting that certain perfusion parameters are specifically contributing to this component, but
533 not the perfusion lag. Overall, the BOLD low-frequency phase behaved as a deoxy Hb-based virtual
534 contrast agent in the present data, leaving a global, but separable noise component for the fMRI
535 analysis.

536 The observation that the velocity on the arterial side exhibits changes alongside respiratory
537 variations is consistent with the findings of previous reports using transcranial Doppler
538 ultrasonography (Malatino *et al.*, 1992; Poulin *et al.*, 1996). During the initial whole-brain CBV
539 increase in response to autoregulatory vasodilation, a sole increase in the inflow should first occur
540 to meet the volume demand. It is reasonable that this effect is absent in the outlet, i.e., the venous
541 side of the gross vasculature, as observed in the current study. The low-frequency phase hence
542 appears to directly reflect the perfusion.

543 This result is compatible with the model that the BOLD lag structure is derived from an axial non-
544 uniformity in the vessels, already present in the inflow (Tong *et al.*, 2018). The diminished
545 magnitude observed in the outlet side of the vasculature also suggests a distinct mechanism of the
546 lag structure, other than CBF increase which creates a larger response in the draining vessels (Krings
547 *et al.*, 1999). It is unclear what proportion of this axial variation is systemic, i.e., originating from the
548 autonomic loops, mediated by peripheral baro- or chemoreceptors. At least, even if the neural
549 activity is contributing to this component creating the sLFO, the resulting lag structure would be
550 mainly of vascular origin. In this work, we focused on non-neuronal mechanisms to account for the
551 BOLD lag structure to the extent possible, in the hope that it may ultimately help achieve a better
552 understanding and modeling of the fMRI signal.

553 **4.1 Source of BOLD LFO signals**

554 Previous studies on sLFO have reported that both Hb species fluctuate, but with varying phase
555 difference that is selectively found in the brain (Obrig *et al.*, 2000; Rayshubskiy *et al.*, 2014;
556 Tgavalekos *et al.*, 2016). The observed fluctuations of total Hb density have been linked to CBV
557 changes (Boas & Dale, 2005; Kennerley *et al.*, 2005; Kim & Ogawa, 2012), but interpretations for
558 that of deoxy-Hb have rarely been provided. Only one series of studies by Fantini and others directly
559 addressed the possible axial variation of blood content including oxygen saturation (Fantini, 2014).
560 In support of the conventional theory, Rayshubskiy and colleagues reported, in their human

561 intraoperative study, slow Hb oscillation correlated with vasomotion in the superficial arteries
562 (Rayshubskiy *et al.*, 2014). However, it remains unclear whether an equivalent vasomotion exists in
563 the non-arterial vessels to fully account for the observed lag structure. It is hence worth considering
564 other sources of deoxy-Hb variation. The concept of vasomotion stems from an active diameter
565 change in the precapillary vessels, driving local velocity fluctuations, termed "flowmotion"
566 (Intaglietta, 1990). This flowmotion can reportedly accompany the fluctuation of local Hct that
567 should directly affect deoxy-Hb density (Fagrell *et al.*, 1980; Hudetz *et al.*, 1999). Another possible
568 source for the deoxy-Hb fluctuations is a change in SaO2 that ranges from 94–98% in the artery
569 (Intaglietta *et al.*, 1996; Collins *et al.*, 2015). For example, the respiration-related BOLD signal
570 component is supposed to be mediated by blood CO_2 level and pH, which also shift the oxygen
571 dissociation curve (Birn *et al.*, 2006; Chang & Glover, 2009*a*). These parameters are considered to
572 fluctuate in the blood as part of the autonomic loop, possibly driving vasomotion, at least in part,
573 which persists even after denervation (Morita *et al.*, 1995). As mentioned above, the phase
574 difference between the two Hb species remains to be elucidated (Sassaroli *et al.*, 2012), but this
575 observation itself substantiates an unstable deoxy-Hb supply in brain tissues. Besides, such a signal
576 component would have escaped detection in NVC studies using trial averaging.

577 A signal origin intrinsic to the flowing blood may, as suggested by Tong and colleagues, thus explain
578 the constant phase difference among signals from different body parts (Tong *et al.*, 2012, 2017). In
579 the literature, an axial variation of the Hct in the brain has indeed been suggested, in relation to
580 both NVC (Kleinschmidt *et al.*, 1996; Siegel *et al.*, 2003; Chen & Pike, 2009) and sLFOs (Fagrell *et al.*,
581 1980; Mayhew *et al.*, 1996). Furthermore, the reduction in T2* LFO amplitude in the venous side
582 can be explained by the high tissue deoxy-Hb density, which probably diminishes the proportional
583 effect of intrinsic deoxy-Hb fluctuations, unless the oxygen consumption is completely coupled to
584 this variation. Importantly, temporal dispersion alone would not fully account for the amplitude
585 reduction, as it was only found in the venous side, despite the fact that the lag structure was
586 tracked both up- and downstream from the global phase. These results provide good contrast with
587 the stable S_0 response, reflecting its insensitivity to oxygen saturation. Although it would be too
588 challenging to incorporate complex rheological parameters, a reconsideration of the constant
589 deoxy-Hb assumption may help improve the BOLD signal modelling.

590 In the hyperventilation condition, we observed a fast response to each ventilation cycle,
591 accompanying blood pressure change. Although the effect of respiratory movement cannot be fully
592 excluded, the spatial pattern in **Supplementary Figure 2B** is not that of a typical motion artifact
593 centered on the brain surface (Krings *et al.*, 2001). In healthy subjects, inhalation increases systemic
594 venous return through decreased intrathoracic pressure, causing elevation of the cardiac output
595 with some delay. In contrast, exhalation is considered to cause CBV increase through elevated
596 cerebral venous pressure. To our knowledge, the timing order of these events has not been studied
597 at the precision of the current data, and further studies are needed to determine the source of this
598 S_0 fluctuation (Yen *et al.*, 2017). The only available clue is the spatial distribution, such as the

interesting anterior-posterior segmentation (resembling the unique "S_0 lag structure" in **Fig. 9a**) or the symmetrical pattern in the deep brain structures. At least, some mechanical effect of the respiratory act on the fluid dynamics likely exists, causing this spatially-heterogeneous S_0 deflection.

4.2 Lag structure as noise

Based on the assumption that the global signal fluctuation is the sum of all variations by NVC, its elimination by GSR has been considered to negatively bias the results (Caballero-Gaudes & Reynolds, 2017). However, as noted by Aguirre and others, there are cases where GSR yields interpretable results even in the absence of global motion artifacts (Aguirre *et al.*, 1998). The rise in popularity of rs-fMRI since 2005 has led to this issue resurfacing in a different form. A variation in GSR, in which the timeseries extracted from a set of regions-of-interest (whole brain, white matter, and cerebrospinal fluid) are removed, has become a *de facto* standard. It is indeed computationally closer to our deperfusioning in that the regional phase difference is somehow tolerated. However, because this practice lacked strong theoretical background (Chang *et al.*, 2009; Liu *et al.*, 2017), currently, the identification and elimination of bodily movements and physiological noise are more widely recommended. There are various approaches to this end, such as simultaneous physiological measurements (Chang & Glover, 2009*b*), as well as data-driven methods that only use fMRI data (Smith *et al.*, 2013). To date, however, objective criteria for distinguishing neural activity from noise components remains an issue (Salimi-Khorshidi *et al.*, 2014).

In the present study, the lag structure was treated as a broadly-distributed structured noise for fMRI. Indeed, it can be substantially eliminated by sophisticated denoising techniques (Aso *et al.*, 2017*a*). However, the specificity of lag mapping in isolating information on a purely vascular origin remains, however, unclear. For example, measurement of velocity changes critically depends on a recursive lag-tracking method, which incorporates the gradual change in LFO over regions (Tong & Frederick, 2014). Adaptation for changes in the waveform that may arise from different paths of the blood is not only theoretically plausible, but was demonstrated to increase the reproducibility of the lag (Aso *et al.*, 2017*a*). However, as the changes in waveform reflect any fluctuation originating either from the vascular anatomy or NVC, removing the whole lag structure may lead to type II errors in the fMRI results. The favorable impacts of the deperfusioning procedure that we observed on the fMRI results are clearly insufficient to prove the advantage of this technique and require further confirmation.

Importantly, the detection of the lag structure itself is dependent on data quality and affected by body movements. This would be the case when a significant head movement results in a synchronized deflection that exceeds the LFO amplitude, thus obscuring the phase variation. However, it can be also questioned if the correlational structure of neural activity is reliably detected from such motion-contaminated data. In general, NVC should have a limited spatial extent and signal magnitude without time-locked averaging (Power *et al.*, 2012). In turn, successful

tracking of a lag structure may even be considered as evidence of "clean" data. Thus, the elimination of this identified lag structure can be a relatively straightforward approach to reduce structured physiological noise (Caballero-Gaudes & Reynolds, 2017).

In conclusion, by investigating various aspects of the BOLD sLFO, we compiled supporting evidence for a component intrinsic to flowing blood that has been a focus of interest in earlier works (Tong *et al.*, 2017). To establish a framework by which the fMRI signal can be fully modeled, more detailed characterization of the lag structure as part of the "global noise" is needed (Glasser *et al.*, 2018).

5 Conflict of Interest

The authors declare that the research was conducted in the absence of any commercial or financial relationships that could be construed as a potential conflict of interest.

6 Author Contributions

All authors provided approval of the final version of the manuscript to be published. TA contributed to concept and design of this research, data analysis and interpretation, and drafting of the manuscript. SU contributed to data acquisition and drafting of the manuscript. SU, HF, and TM contributed to data interpretation and review of the final draft.

7 Funding

This study was supported by Grant-in-Aid for Scientific Research on Innovative Areas (Non-linear Neuro-oscillology: Towards Integrative Understanding of Human Nature, JP15H05875) to T.A. and JP16H06395 and JP16H06397 to T.M. from the Japan Society for the Promotion of Science.

8 Acknowledgments

We would like to thank Editage (www.editage.jp) for English language editing.

9 Data Availability Statement

The datasets analyzed for this study can be provided upon request.

10 References

Aguirre GK, Zarahn E & D'Esposito M (1998). The inferential impact of global signal covariates in functional neuroimaging analyses. *NeuroImage* **8,** 302–306.

Amemiya S, Kunimatsu A, Saito N & Ohtomo K (2013). Cerebral Hemodynamic Impairment: Assessment with Resting-State Functional MR Imaging. *Radiology* **270,** 1–8.

Amemiya S, Takao H, Hanaoka S & Ohtomo K (2016). Global and structured waves of rs-fMRI signal identified as putative propagation of spontaneous neural activity. *NeuroImage* **133,** 331–340.

An H & Lin W (2002). Cerebral oxygen extraction fraction and cerebral venous blood volume measurements using MRI: Effects of magnetic field variation. *Magnetic Resonance in Medicine* **47,** 958–966.

Anderson JS, Druzgal TJ, Lopez-Larson M, Jeong E, Desai K & Yurgelun-Todd D (2011). Network anticorrelations, global regression, and phase-shifted soft tissue correction. *Human brain mapping* **32,** 919–934.

Aso T, Jiang G, Urayama S & Fukuyama H (2017*a*). A Resilient, Non-neuronal Source of the Spatiotemporal Lag Structure Detected by BOLD Signal-Based Blood Flow Tracking. *Frontiers in Neuroscience* **11,** 256.

Aso T, Urayama S & Fukuyama H (2017*b*). Temporal variation of cerebrovascular transit time measured by BOLD-based time lag mapping. In *Proceedings of the 25rd Annual Meeting of ISMRM*. Honolulu.

Birn RM, Diamond JB, Smith M a. & Bandettini P a. (2006). Separating respiratory-variation-related fluctuations from neuronal-activity-related fluctuations in fMRI. *NeuroImage* **31,** 1536–1548.

Birn RM, Murphy K & Bandettini PA (2008). The effect of respiration variations on independent component analysis results of resting state functional connectivity. *Human Brain Mapping* **29,** 740–750.

Blockley NP, Driver ID, Francis ST, Fisher JA & Gowland PA (2011). An improved method for acquiring cerebrovascular reactivity maps. *Magnetic Resonance in Medicine* **65,** 1278–1286.

Boas DA & Dale AM (2005). Simulation study of magnetic resonance imaging–guided cortically constrained diffuse optical tomography of human brain function. *Applied Optics* **44,** 1957.

Buxton RB (2013). The physics of functional magnetic resonance imaging (fMRI). *Reports on Progress in Physics* **76,** 096601.

Byrge L & Kennedy DP (2018). Identifying and characterizing systematic temporally-lagged BOLD artifacts. *NeuroImage* **171,** 376–392.

Caballero-Gaudes C & Reynolds RC (2017). Methods for cleaning the BOLD fMRI signal. *NeuroImage* **154,** 128–149.

Chang C, Cunningham JP & Glover GH (2009). Influence of heart rate on the BOLD signal: The cardiac response function. *NeuroImage* **44,** 857–869.

Chang C & Glover GH (2009*a*). Relationship between respiration, end-tidal CO2, and BOLD signals in resting-state fMRI. *NeuroImage* **47,** 1381–1393.

Chang C & Glover GH (2009*b*). Effects of model-based physiological noise correction on default mode network anti-correlations and correlations. *NeuroImage* **47,** 1448–1459.

Chen JJ & Pike GB (2009). BOLD-specific cerebral blood volume and blood flow changes during neuronal activation in humans. *NMR in biomedicine* **22,** 1054–1062.

Christen T, Jahanian H, Ni WW, Qiu D, Moseley ME & Zaharchuk G (2015). Noncontrast mapping of arterial delay and functional connectivity using resting-state functional MRI: A study in Moyamoya patients. *Journal of Magnetic Resonance Imaging* **41,** 424–430.

Cohen ER, Ugurbil K & Kim S-G (2002). Effect of basal conditions on the magnitude and dynamics of

the blood oxygenation level-dependent fMRI response. *Journal of cerebral blood flow and metabolism: official journal of the International Society of Cerebral Blood Flow and Metabolism* **22,** 1042–1053.

Collins J-A, Rudenski A, Gibson J, Howard L & O'Driscoll R (2015). Relating oxygen partial pressure, saturation and content: the haemoglobin-oxygen dissociation curve. *Breathe (Sheffield, England)* **11,** 194–201.

Dresel C, Castrop F, Haslinger B, Wohlschlaeger AM, Hennenlotter A & Ceballos-Baumann AO (2005). The functional neuroanatomy of coordinated orofacial movements: Sparse sampling fMRI of whistling. *NeuroImage* **28,** 588–597.

Erdoğan SB, Tong Y, Hocke LM, Lindsey KP & Blaise deB Frederick (2016). Correcting for Blood Arrival Time in Global Mean Regression Enhances Functional Connectivity Analysis of Resting State fMRI-BOLD Signals. *Frontiers in human neuroscience* **10,** 311.

Fagrell B, Fronek A & Intaglietta M (1977). A microscope-television system for studying flow velocity in human skin capillaries. *The American journal of physiology* **233,** H318-21.

Fagrell B, Intaglietta M & Ostergren J (1980). Relative hematocrit in human skin capillaries and its relation to capillary blood flow velocity. *Microvascular research* **20,** 327–335.

Fantini S (2014). Dynamic model for the tissue concentration and oxygen saturation of hemoglobin in relation to blood volume, flow velocity, and oxygen consumption: Implications for functional neuroimaging and coherent hemodynamics spectroscopy (CHS). *NeuroImage* **85,** 202–221.

Feinberg D a, Moeller S, Smith SM, Auerbach E, Ramanna S, Gunther M, Glasser MF, Miller KL, Ugurbil K & Yacoub E (2010). Multiplexed echo planar imaging for sub-second whole brain FMRI and fast diffusion imaging. *PloS one* **5,** e15710.

Freire L & Mangin JF (2001). Motion correction algorithms may create spurious brain activations in the absence of subject motion. *NeuroImage* **14,** 709–722.

Friston KJ, Glaser DE, Henson RNA, Kiebel S, Phillips C & Ashburner J (2002). Classical and Bayesian inference in neuroimaging: Applications. *NeuroImage* **16,** 484–512.

Giller CA, Hatab MR & Giller AM (1999). Oscillations in cerebral blood flow detected with a transcranial Doppler index. *Journal of cerebral blood flow and metabolism: official journal of the International Society of Cerebral Blood Flow and Metabolism* **19,** 452–459.

Glasser MF, Coalson TS, Bijsterbosch JD, Harrison SJ, Harms MP, Anticevic A, Van Essen DC & Smith SM (2018). Using temporal ICA to selectively remove global noise while preserving global signal in functional MRI data. *NeuroImage* **181,** 692–717.

Guyton AC & Harris JW (1951). Pressoreceptor-autonomic oscillation; a probable cause of vasomotor waves. *The American journal of physiology* **165,** 158–166.

Herman P, Sanganahalli BG & Hyder F (2009). Multimodal Measurements of Blood Plasma and Red Blood Cell Volumes during Functional Brain Activation. *Journal of Cerebral Blood Flow & Metabolism* **29,** 19–24.

Hillman EMC (2014). Coupling Mechanism and Significance of the BOLD Signal: A Status Report. *Annual Review of Neuroscience* **37,** 161–181.

Hoge R, Atkinson J, Gill B, Crelier G & Marrett S (1999). Investigation of BOLD signal dependence on cerebral blood flow and oxygen consumption: The …. *Magnetic Resonance in Medicine* **863,** 849–863.

Hoiland RL, Tymko MM, Bain AR, Wildfong KW, Monteleone B & Ainslie PN (2016). Carbon dioxide-mediated vasomotion of extra-cranial cerebral arteries in humans: a role for prostaglandins? *J Physiol* **594,** 3463–3481.

Hudetz a G, Wood JD, Biswal BB, Krolo I & Kampine JP (1999). Effect of hemodilution on RBC velocity, supply rate, and hematocrit in the cerebral capillary network. *Journal of applied physiology (Bethesda, Md: 1985)* **87,** 505–509.

Intaglietta M (1990). Vasomotion and flowmotion: physiological mechanisms and clinical evidence. *Vascular Medicine Review* **1,** 101–112.

Intaglietta M, Johnson PC & Winslow RM (1996). Microvascular and tissue oxygen distribution. *Cardiovascular research* **32,** 632–643.

Julien C (2006). The enigma of Mayer waves: Facts and models. *Cardiovascular research* **70,** 12–21.

Katura T, Tanaka N, Obata A, Sato H & Maki A (2006). Quantitative evaluation of interrelations between spontaneous low-frequency oscillations in cerebral hemodynamics and systemic cardiovascular dynamics. *NeuroImage* **31,** 1592–1600.

Kennerley AJ, Berwick J, Martindale J, Johnston D, Papadakis N & Mayhew JE (2005). Concurrent fMRI and Optical Measures for the Investigation of the Hemodynamic Response Function. **365,** 354–365.

Khalil AA, Villringer K, Filleböck V, Hu J-Y, Rocco A, Fiebach JB & Villringer A (2018). Non-invasive monitoring of longitudinal changes in cerebral hemodynamics in acute ischemic stroke using BOLD signal delay. *Journal of Cerebral Blood Flow & Metabolism*0271678X1880395.

Killip T (1962). Oscillation of blood flow and vascular resistance during Mayer waves. *Circulation research* **11,** 987–993.

Kim JH & Ress D (2016). Arterial impulse model for the BOLD response to brief neural activation. *NeuroImage* **124,** 394–408.

Kim S-G & Ogawa S (2012). Biophysical and physiological origins of blood oxygenation level-dependent fMRI signals. *Journal of Cerebral Blood Flow & Metabolism* **32,** 1188–1206.

Kleinschmidt A, Obrig H, Requardt M, Merboldt K-D, Dirnagl U, Villringer A & Frahm J (1996). Simultaneous Recording of Cerebral Blood Oxygenation Changes during Human Brain Activation by Magnetic Resonance Imaging and Near-Infrared Spectroscopy. *Journal of Cerebral Blood Flow & Metabolism* **16,** 817–826.

Krings T, Erberich SG, Roessler F, Reul J & Thron A (1999). MR blood oxygenation level-dependent signal differences in parenchymal and large draining vessels: implications for functional MR imaging. *AJNR American journal of neuroradiology* **20,** 1907–1914.

Krings T, Reinges MHT, Erberich S, Kemeny S, Rohde V, Spetzger U, Korinth M, Willmes K, Gilsbach JM & Thron A (2001). Functional MRI for presurgical planning: problems, artefacts, and solution strategies. *J Neurol Neurosurg Psychiatry* **70,** 749.

Kumar V, Croxson PL & Simonyan K (2016). Structural Organization of the Laryngeal Motor Cortical

Network and Its Implication for Evolution of Speech Production. *Journal of Neuroscience* **36,** 4170–4181.

Kundu P, Inati SJ, Evans JW, Luh W-M & Bandettini PA (2012). Differentiating BOLD and non-BOLD signals in fMRI time series using multi-echo EPI. *NeuroImage* **60,** 1759–1770.

Liu TT, Nalci A & Falahpour M (2017). The global signal in fMRI: Nuisance or Information? *NeuroImage* **150,** 213–229.

Lv Y, Margulies DS, Cameron Craddock R, Long X, Winter B, Gierhake D, Endres M, Villringer K, Fiebach J & Villringer A (2013). Identifying the perfusion deficit in acute stroke with resting-state functional magnetic resonance imaging. *Annals of Neurology* **73,** 136–140.

Malatino LS, Bellofiore S, Costa MP, Lo Manto G, Finocchiaro F & Di Maria GU (1992). Cerebral blood flow velocity after hyperventilation-induced vasoconstriction in hypertensive patients. *Stroke* **23,** 1728–1732.

Mayhew JEW, Askew S, Zheng Y, Porrill J, Westby GWMW, Redgrave P, Rector DM & Harper RM (1996). Cerebral Vasomotion: A 0.1-Hz Oscillation in Reflected Light Imaging of Neural Activity. *NeuroImage* **4,** 183–193.

Mazaika PK, Hoeft F, Glover GH & Reiss AL (2009). Methods and Software for fMRI Analysis of Clinical Subjects. *NeuroImage* **47,** S58.

McKay LC, Adams L, Frackowiak RSJ & Corfield DR (2008). A bilateral cortico-bulbar network associated with breath holding in humans, determined by functional magnetic resonance imaging. *NeuroImage* **40,** 1824–1832.

Morita Y, Hardebo JE & Bouskela E (1995). Influence of cerebrovascular sympathetic, parasympathetic, and sensory nerves on autoregulation and spontaneous vasomotion. *Acta Physiol Scand* **154,** 121–130.

Murphy K, Birn RM & Bandettini PA (2013). Resting-state fMRI confounds and cleanup. *NeuroImage* **80,** 349–359.

Murphy K, Harris AD & Wise RG (2011). Robustly measuring vascular reactivity differences with breath-hold: Normalising stimulus-evoked and resting state BOLD fMRI data. *NeuroImage* **54,** 369–379.

Ni L, Li J, Li W, Zhou F, Wang F, Schwarz CG, Liu R, Zhao H, Wu W, Zhang X, Li M, Yu H, Zhu B, Villringer A, Zang Y, Zhang B, Lv Y & Xu Y (2017). The value of resting-state functional MRI in subacute ischemic stroke: comparison with dynamic susceptibility contrast-enhanced perfusion MRI. *Scientific Reports* **7,** 41586.

Nikulin V V, Fedele T, Mehnert J, Lipp A, Noack C, Steinbrink J & Curio G (2014). Monochromatic Ultra-Slow (~0.1Hz) Oscillations in the human electroencephalogram and their relation to hemodynamics. *NeuroImage* **97,** 71–80.

Nishida S, Aso T, Takaya S, Takahashi Y, Kikuchi T, Funaki T, Yoshida K, Okada T, Kunieda T, Togashi K, Fukuyama H & Miyamoto S (2018). Resting-state Functional Magnetic Resonance Imaging Identifies Cerebrovascular Reactivity Impairment in Patients With Arterial Occlusive Diseases: A Pilot Study. *Neurosurgery*; DOI: 10.1093/neuros/nyy434.

Obrig H, Neufang M, Wenzel R, Kohl M, Steinbrink J, Einhäupl K & Villringer A (2000). Spontaneous

Low Frequency Oscillations of Cerebral Hemodynamics and Metabolism in Human Adults. *NeuroImage* **12,** 623–639.

Ogawa S, Menon RS, Kim SG & Ugurbil K (1998). On the characteristics of functional magnetic resonance imaging of the brain. *AnnuRevBiophysBiomolStruct* **27,** 447–474.

Pattinson KTS, Governo RJ, MacIntosh BJ, Russell EC, Corfield DR, Tracey I & Wise RG (2009). Opioids Depress Cortical Centers Responsible for the Volitional Control of Respiration. *Journal of Neuroscience* **29,** 8177–8186.

Poline JB, Worsley KJ, Evans AC & Friston KJ (1997). Combining spatial extent and peak intensity to test for activations in functional imaging. *NeuroImage* **5,** 83–96.

Posse S, Wiese S, Gembris D, Mathiak K, Kessler C, Grosse-Ruyken ML, Elghahwagi B, Richards T, Dager SR & Kiselev VG (1999). Enhancement of BOLD-contrast sensitivity by single-shot multi-echo functional MR imaging. *Magnetic resonance in medicine* **42,** 87–97.

Poulin MJ, Liang PJ & Robbins PA (1996). Dynamics of the cerebral blood flow response to step changes in end-tidal PCO2 and PO2 in humans. *Journal of Applied Physiology* **81,** 1084–1095.

Power JD, Barnes K a., Snyder AZ, Schlaggar BL & Petersen SE (2012). Spurious but systematic correlations in functional connectivity MRI networks arise from subject motion. *NeuroImage* **59,** 2142–2154.

Power JD, Plitt M, Laumann TO & Martin A (2017). Sources and implications of whole-brain fMRI signals in humans. *NeuroImage* **146,** 609–625.

Radna RJ & MacLean PD (1981). Vagal elicitation of respiratory-type and other unit responses in striopallidum of squirrel monkeys. *Brain Research* **213,** 29–44.

Rayshubskiy A, Wojtasiewicz TJ, Mikell CB, Bouchard MB, Timerman D, Youngerman BE, McGovern RA, Otten ML, Canoll P, McKhann GM & Hillman EMC (2014). Direct, intraoperative observation of ~0.1Hz hemodynamic oscillations in awake human cortex: Implications for fMRI. *NeuroImage* **87,** 323–331.

Rostrup E, Knudsen GM, Law I, Holm S, Larsson HBW & Paulson OB (2005). The relationship between cerebral blood flow and volume in humans. *NeuroImage* **24,** 1–11.

Salimi-Khorshidi G, Douaud G, Beckmann CF, Glasser MF, Griffanti L & Smith SM (2014). Automatic denoising of functional MRI data: Combining independent component analysis and hierarchical fusion of classifiers. *NeuroImage* **90,** 449–468.

Sassaroli A, Pierro M, Bergethon PR & Fantini S (2012). Low-frequency spontaneous oscillations of cerebral hemodynamics investigated with near-infrared spectroscopy: A review. *IEEE Journal on Selected Topics in Quantum Electronics* **18,** 1478–1492.

Satow T, Aso T, Nishida S, Komuro T, Ueno T, Oishi N, Nakagami Y, Odagiri M, Kikuchi T, Yoshida K, Ueda K, Kunieda T, Murai T, Miyamoto S & Fukuyama H (2017). Alteration of Venous Drainage Route in Idiopathic Normal Pressure Hydrocephalus and Normal Aging. *Frontiers in Aging Neuroscience*; DOI: 10.3389/fnagi.2017.00387.

Satterthwaite TD, Elliott MA, Gerraty RT, Ruparel K, Loughead J, Calkins ME, Eickhoff SB, Hakonarson H, Gur RC, Gur RE & Wolf DH (2013). An improved framework for confound regression and filtering for control of motion artifact in the preprocessing of resting-state

functional connectivity data. *NeuroImage* **64,** 240–256.

Siegel AM, Culver JP, Mandeville JB & Boas DA (2003). Temporal comparison of functional brain imaging with diffuse optical tomography and fMRI during rat forepaw stimulation. *Physics in medicine and biology* **48,** 1391–1403.

Simonyan K & Jürgens U (2003). Efferent subcortical projections of the laryngeal motorcortex in the rhesus monkey. *Brain Research* **974,** 43–59.

Smith SM et al. (2013). Resting-state fMRI in the Human Connectome Project. *NeuroImage* **80,** 144–168.

Smith SM, Jenkinson M, Woolrich MW, Beckmann CF, Behrens TEJ, Johansen-Berg H, Bannister PR, De Luca M, Drobnjak I, Flitney DE, Niazy RK, Saunders J, Vickers J, Zhang Y, De Stefano N, Brady JM & Matthews PM (2004). Advances in functional and structural MR image analysis and implementation as FSL. *NeuroImage* **23 Suppl 1,** S208-19.

Taylor Webb J, Ferguson M a., Nielsen J a. & Anderson JS (2013). BOLD granger causality reflects vascular anatomy. *PLoS ONE* **8,** 1–19.

Tgavalekos KT, Kainerstorfer JM, Sassaroli A & Fantini S (2016). Blood-pressure-induced oscillations of deoxy- and oxyhemoglobin concentrations are in-phase in the healthy breast and out-of-phase in the healthy brain. *Journal of Biomedical Optics* **21,** 101410.

Thomas DL, Lythgoe MF, Pell GS, Calamante F & Ordidge RJ (2000). The measurement of diffusion and perfusion in biological systems using magnetic resonance imaging. *Physics in medicine and biology* **45,** R97-138.

Tian F, Niu H, Khan B, Alexandrakis G, Behbehani K & Liu H (2011). Enhanced Functional Brain Imaging by Using Adaptive Filtering and a Depth Compensation Algorithm in Diffuse Optical Tomography. *IEEE Transactions on Medical Imaging* **30,** 1239–1251.

Tong Y & Frederick B deB (2014). Tracking cerebral blood flow in BOLD fMRI using recursively generated regressors. *Human brain mapping* **35,** 5471–5485.

Tong Y, Hocke LM, Licata SC & Frederick B deB (2012). Low-frequency oscillations measured in the periphery with near-infrared spectroscopy are strongly correlated with blood oxygen level-dependent functional magnetic resonance imaging signals. *Journal of biomedical optics* **17,** 106004.

Tong Y, Lindsey KP, Hocke LM, Vitaliano G, Mintzopoulos D & Frederick B deB (2017). Perfusion information extracted from resting state functional magnetic resonance imaging. *Journal of cerebral blood flow and metabolism: official journal of the International Society of Cerebral Blood Flow and Metabolism* **37,** 564–576.

Tong Y, Yao JF, Chen JJ & Frederick B deB (2018). The resting-state fMRI arterial signal predicts differential blood transit time through the brain. *Journal of cerebral blood flow and metabolism: official journal of the International Society of Cerebral Blood Flow and Metabolism*271678X17753329.

Tuunanen PI & Kauppinen RA (2006). Effects of oxygen saturation on BOLD and arterial spin labelling perfusion fMRI signals studied in a motor activation task. *NeuroImage* **30,** 102–109.

Willie CK, Tzeng Y-C, Fisher JA & Ainslie PN (2014). Integrative regulation of human brain blood flow:

Integrative regulation of human brain blood flow. *The Journal of Physiology* **592,** 841–859.

Winder AT, Echagarruga C, Zhang Q & Drew PJ (2017). Weak correlations between hemodynamic signals and ongoing neural activity during the resting state. *Nature neuroscience* **20,** 1761–1769.

Wise RG, Ide K, Poulin MJ & Tracey I (2004). Resting fluctuations in arterial carbon dioxide induce significant low frequency variations in BOLD signal. *NeuroImage* **21,** 1652–1664.

Wu CW, Gu H, Zou Q, Lu H, Stein EA & Yang Y (2012). TE-dependent spatial and spectral specificity of functional connectivity. *NeuroImage* **59,** 3075–3084.

Yablonskiy DA & Haacke EM (1994). Theory of NMR signal behavior in magnetically inhomogeneous tissues: the static dephasing regime. *Magnetic resonance in medicine* **32,** 749–763.

Yen CC-C, Papoti D & Silva AC (2017). Investigating the spatiotemporal characteristics of the deoxyhemoglobin-related and deoxyhemoglobin-unrelated functional hemodynamic response across cortical layers in awake marmosets. *NeuroImage* **7,** 83–88.

Zhu DC, Tarumi T, Khan MA & Zhang R (2015). Vascular coupling in resting-state fMRI: evidence from multiple modalities. *Journal of cerebral blood flow and metabolism: official journal of the International Society of Cerebral Blood Flow and Metabolism* **35,** 1910–1920.